Transactions, SMiRT-22
San Francisco, California, USA - August 18-23, 2013
Division VI

In-Plane Shear Behavior of Nuclear Power Plant Wall Elements with High-Strength Reinforcing Bars

Gwang-Min Bae[1], Giorgio T. Proestos[2], Seong-Cheol Lee[3], Evan C. Bentz[4], Michael P. Collins[5], and Jae-Yeol Cho[6]

[1] M.A.Sc. Candidate, Dept. of Civil and Environmental Engineering, Seoul National University, Seoul, Korea
[2] M.A.Sc. Candidate, Dept. of Civil Engineering, University of Toronto, Toronto, ON, Canada
[3] Assistant Professor, Dept. of NPP Engineering, KEPCO International Nuclear Graduate School (KINGS), Ulsan, Korea
[4] Associate Professor, Dept. of Civil Engineering, University of Toronto, Toronto, ON, Canada
[5] University Professor, Dept. of Civil Engineering, University of Toronto, Toronto, ON, Canada
[6] Associate Professor, Dept. of Civil and Environmental Engineering, Seoul National University, Seoul, Korea (jycho@snu.ac.kr)

ABSTRACT

This paper presents the results of six reinforced concrete shell element tests representative of one-third scale Nuclear Power Plant (NPP) wall elements, which were tested to failure in combined membrane shear and axial stresses. The elements were monotonically loaded until failure and the results were compared to predictions from the Modified Compression Field Theory (MCFT). The ultimate load was accurately predicted with a mean test to predicted ratio of 0.992 and a coefficient of variation of 5.38%. The shear strains at peak stress were also accurately predicted with a mean test to predicted ratio of 0.987 and a coefficient of variation of 8.10%. The effects of using high-strength reinforcing bars, while maintaining the ρf_y ratios were compared. The results showed that using high-strength reinforcing bars reduced the normalized strength of the specimens. The effect of biaxial tension and biaxial compression on the shear behavior was also compared. The members subjected to pure shear failed by crushing of the concrete after the transverse steel yielded. As predicted, the members with biaxial tension failed at lower loads by yielding in both directions, followed by crushing of the concrete. The tests with biaxial compression failed at higher loads by crushing, just as the transverse steel began to yield. This paper presents a summary of the six tests conducted and member behavior is compared to MCFT predictions.

INTRODUCTION

In recent years, design codes have implemented compression field approaches for the design of structures subjected to shear. In particular, the Modified Compression Field Theory [Vecchio and Collins (1986)] has become the basis of the shear provisions in AASHTO, CSA A23.3 and EC2 [Bentz and Collins (2006)]. It is expected that codes used for the design of NPP structures, such as ASME, ACI 349 and ACI 318, will adopt MCFT based provisions in the near future [CSA A23.3-04 (2004), ACI Committee 318 (2008), BS EN 1992-1-1:2004 (2004)]. In NPP structures, such as nuclear containment facilities, high levels of conservatism and cautiousness have led to code provisions that may result in uneconomical designs. For instance, high-strength reinforcing bars have not traditionally been permitted.

NPP structures are subjected to a variety of loading conditions. In the event of a nuclear incident, pressures inside the power plant build, resulting in large biaxial tensions in the facility walls. Furthermore, seismic events will induce large shears combined with axial stresses near the base of nuclear containment structures. For these reasons, pure membrane shear, membrane shear combined with biaxial tension and membrane shear combined with biaxial compression tests were conducted. The detailing of the reinforced

concrete members and membrane shear to axial stress ratios were selected to match typical NPP designs near the base of the containment facility wall.

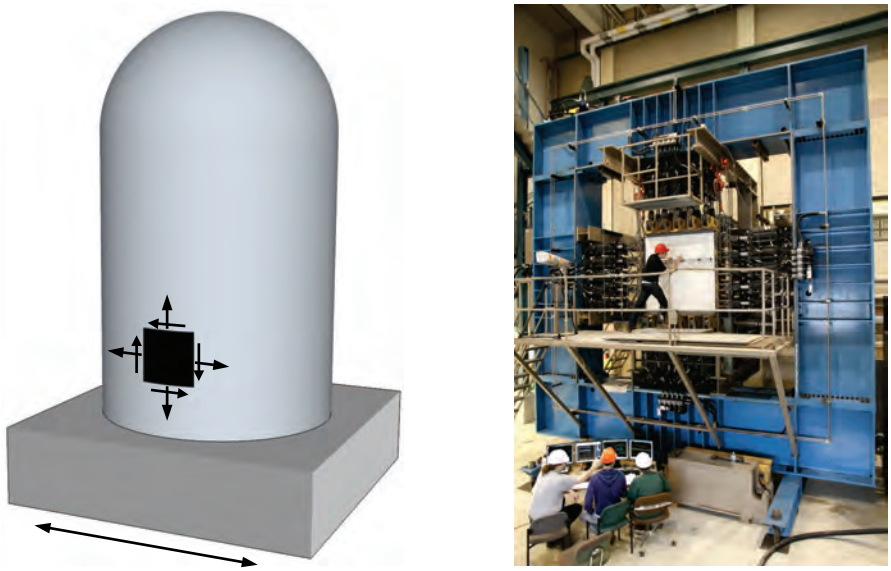

Figure 1. NPP wall element subjected to shear (left) and Shell Element Tester (right).

The MCFT predicts that for heavily reinforced structures, the ρf_y ratio in both directions is an important factor in determining the ultimate shear strength of reinforced concrete members. However, it is important to appreciate that when the same ρf_y is maintained but the steel strength is increased, specimens will have larger steel strains. These larger steel strains will result in more compression softening and lower tensile stresses in the cracked concrete, which reduces member strength. Similarly, the MCFT predicts that crack widths will be larger when using higher steel strengths for members with similar ρf_y ratios. This phenomenon is known as the strain effect in shear.

EXPERIMENTAL PROGRAM

This experimental program is aimed at investigating the influence of high-strength reinforcing bars on the shear response of reinforced concrete NPP elements. Six reinforced concrete shell elements, 1626 x 1626 mm square and 355 mm thick (64 x 64 x 14 in.) were constructed using concrete strengths of approximately 35-40 MPa (5080-5660 psi) (see Fig. 2). The first three shells contained 2.09% of reinforcement in the longitudinal (x) direction and 1.35% of reinforcement in the transverse (y) direction. This steel was specified to have a nominal yield stress of 420 MPa (test series 'A'). The remaining three members were reinforced with 1.56% of reinforcement in the longitudinal direction and 1.04% of reinforcement in the transverse direction. This steel was specified to have a nominal yield stress of 550 MPa (test series 'B'). No out-of-plane (z) reinforcement was provided. These six specimens are six of twelve being tested in the experimental program.

These orthogonal arrangements of steel are oriented at 45 degrees to the direction of applied principle stresses (see Fig. 3). The reduction in percentage of steel in the second set of specimens corresponds to the increase in strength of the steel (i.e. 420 MPa / 550 MPa). For each configuration, one of the specimens was subjected to pure membrane shear (PS), one was subjected to shear and biaxial tension (SBT) and one was subjected to shear and biaxial compression (SBC). The ratio of axial stress to

shear stress was ± 0.4:1. The detailing and loading conditions were chosen to represent one-third scale wall elements near the base of NPP containment structures.

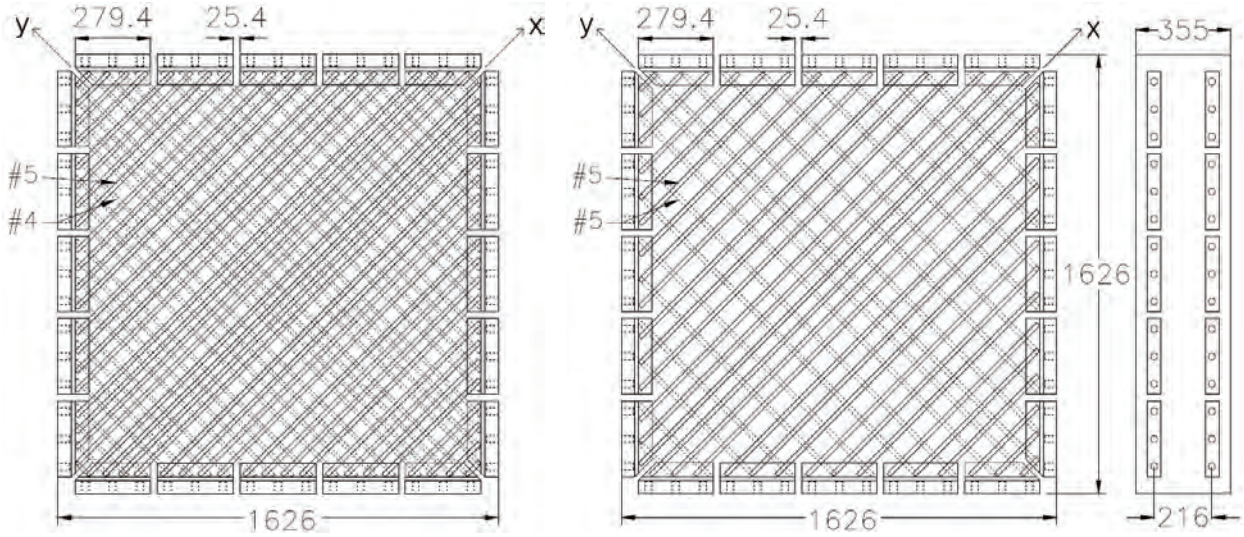

Figure 2. A series (left) and B series (right) specimen details (mm).

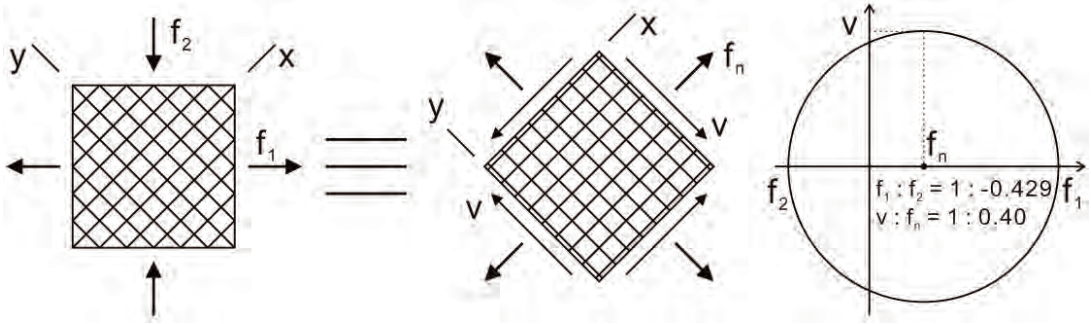

Figure 3. Applied loads and Mohr's circle transformation.

Table 1: Test variables.

Shell	f_{cu} (MPa)	f_{xy} (MPa)	f_{yy} (MPa)	ρ_x (%)	ρ_y (%)	$\rho_x f_{yx}$ (MPa)	$\rho_y f_{yy}$ (MPa)	f_n / v	Remarks
N420A-PS	35.2	448	477	2.09	1.35	9.36	6.44	0	Reference Specimens
N420A-SBT								+0.4	
N420A-SBC								–0.4	
N550B-PS		631	631	1.56	1.04	9.84	6.56	0	Increased f_y with ρf_y maintained in both directions
N550B-SBT	39.6							+0.4	
N550B-SBC								–0.4	

Note: a_g = 20 mm, 1 MPa = 145.0 psi

The specimens were tested in the University of Toronto's Shell Element Tester. This tester has 60 actuators (40 in-plane and 20 out-of-plane) that are controlled with a FlexTest® Controller. Three in-plane actuators and three out-of-plane actuators were held at zero displacement and pinned the structure against rigid body translation. The remaining 17 out-of-plane actuators were commanded to act as stiff springs to restrain out-of-plane movement; all other control channels were force controlled. The specimen was connected to the actuators through loading yokes that were bolted to steel blocks cast in the concrete. The reinforcing bars were welded to these blocks. The 20 vertical actuators induced principle compressive stresses and the 20 horizontal actuators induced principle tensile stresses to the members. From the Mohr's circle transformation, on the 45-degree plane, in the direction of reinforcement, the elements were subjected to principle shear stress (see Fig. 3).

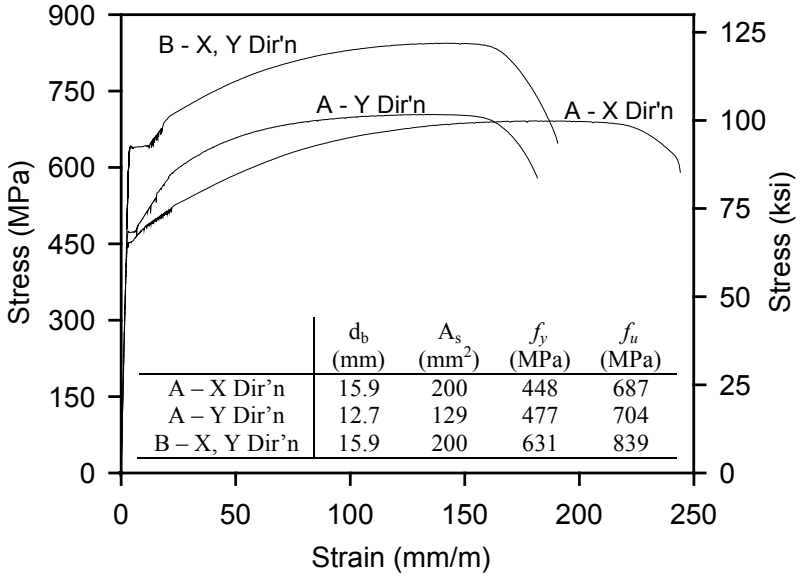

	d_b (mm)	A_s (mm^2)	f_y (MPa)	f_u (MPa)
A – X Dir'n	15.9	200	448	687
A – Y Dir'n	12.7	129	477	704
B – X, Y Dir'n	15.9	200	631	839

Figure 4. Measured properties of reinforcement.

Table 1 provides a summary of the experimental program and includes the shell element names, applied loading ratios (where axial tension is positive and axial compression is negative), concrete strengths and steel strengths, while Fig. 4 shows the stress-strain response of the reinforcing bars used. N420A-PS through N550B-PS were cast from the same batch of concrete; N550B-SBT and N550B-SBC were cast from a second batch of concrete. Testing occurred between 121 to 190 days from the cast date. The tests were conducted by increasing the shear in increments of 0.1 MPa. At regular intervals, and just before failure, the testing was halted and the load was reduced by 10% so that photos could be taken and cracks could be safely marked and measured. The tests were intended to be monotonic. The out-of-plane alignment needed to be adjusted for N420A-PS, N420A-SBC and N550B-PS. These specimens were brought to zero load to adjust the position and then reloaded. No degradation was observed. After failure, N420A-SBT was cycled in an attempt to obtain the post peak response of the member.

The reinforced concrete members were instrumented with six linearly varying differential transducers (LVDTs): 2 horizontal, 2 vertical and 2 diagonal, on both faces. A three-dimensional position scanner was used to determine the location of 35 light emitting diode (LED) targets mounted on the specimen. 16 strain gauges were attached to several reinforcing bars and were cast into the concrete. 40 load cells were used to determine the imposed stress state while the LVDTs and LEDs were used to determine the strain state of the members.

EXPERIMENTAL OBSERVATIONS

Table 2 provides a summary of the key observations for each test. N420A-SBT and N550B-SBT failed by biaxial yielding of the steel followed by crushing of the concrete. These specimens failed relatively slowly before crushing and demonstrated significant ductility. In particular, N550B-SBT was able to maintain significant loads until approximately 48 mm/m of shear strain. N420A-SBC and N550B-SBC failed by crushing of the concrete just as the transverse steel began to yield at the cracks. For these specimens, failure was brittle with the load carrying capacity dropping quickly after the peak load. N420A-PS failed by yielding the transverse steel followed by crushing of the concrete just as the longitudinal steel began to yield. N550B-PS failed by yielding of the transverse reinforcement followed by crushing of the concrete.

For these loading ratios, it can be seen the addition of biaxial tension reduces the strength of the specimens and changes the failure mechanism, resulting in a more ductile response compared to similar specimens tested in pure shear. The addition of biaxial compression increases the strength of the members, even though they were governed by crushing of the concrete [Liping, Bentz and Collins (2011)]. The axial compression reduces the steel strains and in turn reduces the negative effects of compression softening allowing the concrete to carry higher stresses before crushing. Similarly, as the tensile strains in the member increase, less tension can be transmitted in the concrete between the cracks. This dependence on the strain state is known as the strain effect in shear [Collins, Bentz and Sherwood (2008)].

Table 2: Summary of experimental observations.

Shell	f_n/v	f_{cu} (MPa)	Experimental observations							MCFT predictions		v_u Test/ Predicted
			v_{cr} (MPa)	v_u (MPa)	f_{nu} (MPa)	w_{max} (mm)	Strains at v_u (mm/m)			v_u (MPa)	$\gamma_{xy,\,u}$ (mm/m)	
							ε_x	ε_y	γ_{xy}			
N420A-PS	0	35.2	2.10	7.70	0	1.20	2.81	5.81	10.95	7.80	11.33	0.987
N420A-SBT	+0.4		1.60	5.87	+2.35	1.00	3.28	13.9	17.34	5.56	17.17	1.057
N420A-SBC	–0.4		3.17	9.56	–3.82	0.65	1.68	2.42	7.09	10.55	7.61	0.906
N550B-PS	0		2.01	7.68	0	1.40	2.86	5.54	9.64	7.85	10.30	0.978
N550B-SBT	+0.4	39.6	1.30	5.97	+2.39	1.40	3.62	15.6	21.7	5.73	19.00	1.040
N550B-SBC	–0.4		2.78	10.47	–4.19	1.20	2.74	3.27	8.26	10.64	8.77	0.984

For some tests, N420A-SBT and N550B-SBT in particular, significant post peak data were obtained. This was possible because once a control limit was triggered the system unloaded the specimen over several seconds. Since the data acquisition systems were able to capture data at 10 Hz, credible data was collected. This controlled unloading provides an ability to capture post peak response if the failure occurs slowly enough. For members that fail quickly it was difficult to capture the post peak response during unloading.

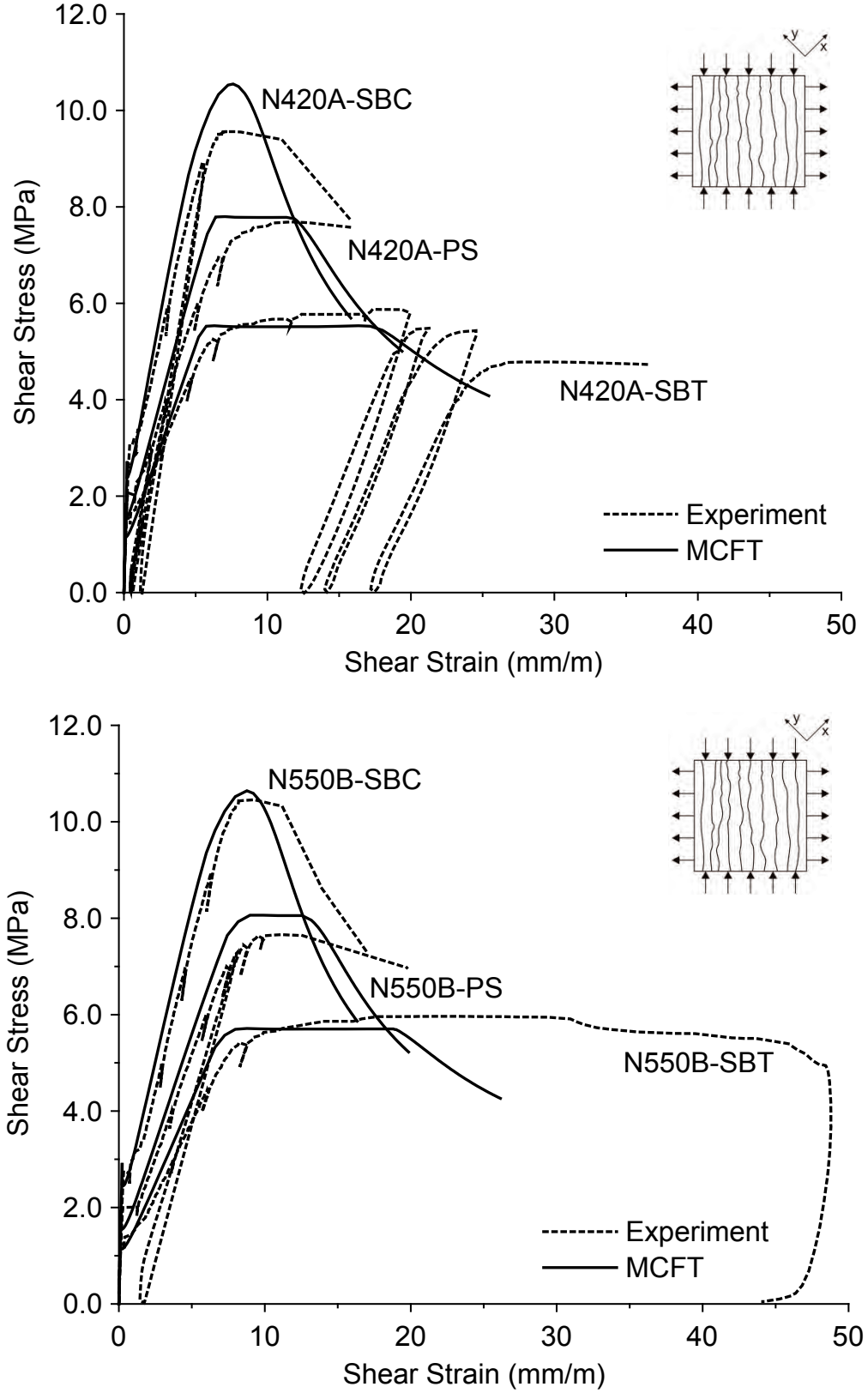

Figure 5. Shear stress-strain response, A series (top) and B series (bottom).

The program Membrane-2012 was used to generate the MCFT predictions for the reinforced concrete members [Bentz (2012)]. The same constitutive relationships as shown in Fig. 6 were used for the analysis with the exception that a modified Popovics formulation was used for the concrete stress strain response [Collins and Mitchell (1991)] and the response of the steel included strain hardening. The mean test to predicted ratio for the ultimate load is 0.992 with a coefficient of variation of 5.38%. The shear strains at peak stress are also accurately predicted by the MCFT with a mean test to predicted ratio of 0.987 and a coefficient of variation of 8.10%. Also, at peak stress the test to predicted ratio for the longitudinal strains is 0.896 with a coefficient of variation of 13.37% and is 1.248 with a coefficient of variation of 20.15% for the transverse strains. This agreement suggests that the compression softening phenomena, which will govern ultimate strains, is accurately captured.

The peak shear stress achieved by N420A-PS and N550B-PS is nearly identical, however the amount of steel in each direction is larger for the N550B-PS member. The reason that the N550B-PS specimen did not achieve higher shear strength is because of the strain effect in shear. Since the concrete strengths and ρf_y ratios both change for the SBT and SBC specimens, it is more difficult to directly observe the strain effect. Membrane-2012 predicts the peak strength of N420A-SBC to be 10.55 MPa, if the concrete strength and the ρf_y ratio is maintained but the yield stress of the reinforcement is increased to 631 MPa, the predicted peak strength decreases to 9.75 MPa, nearly an 8% reduction in strength. Also, the crack widths are larger for members with higher strength steel, as was observed in the tests (see table 2). This strain effect would be more evident if the amount of reinforcement was lower and if the amount of reinforcement in the longitudinal and transverse directions differed significantly.

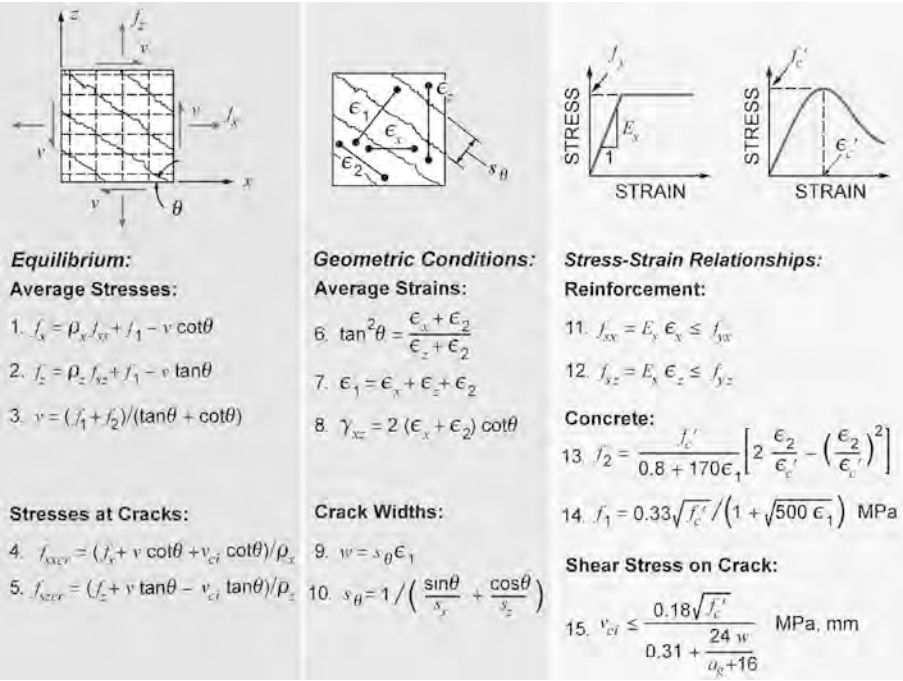

Figure 6. Equations of MCFT.

The cracking load for each specimen varied because different loading ratios and concrete strengths were used, except N420A-PS and N550B-PS, which cracked at nearly the same stress since they were cast from the same batch of concrete and were subjected to the same stress state. The MCFT reasonably captured the cracking loads of the members with a mean test to predicted ratio of 1.066 and a coefficient of variation of 10.45%. This coefficient of variation is good considering the cracking load depends on the tensile strength of the concrete, which is highly variable. The MCFT predicts that the two specimens cast from the second batch of concrete should crack at higher stresses than those cast from the

first batch because the concrete has a higher compressive strength. However, both N550B-SBT and N550B-SBC cracked at lower stresses than their lower strength concrete counterparts. This reduction in cracking stress is likely a result of more shrinkage in the second batch of concrete in comparison to the first. Since these specimens were tested over 121 days from casting, shrinkage was significant and affected the cracking strength.

For the specimens tested in pure shear the cracked elastic stiffness was accurately predicted. In this range, the strains were under predicted by a constant value. This shift is likely due to shrinkage in the concrete. N420A-PS and N550B-PS exhibit more nonlinearity near the ultimate load than is predicted by the MCFT. This nonlinearity may be caused by the local nonlinearity (e.g. at a crack and between loading plates near the boundaries of the specimen), which does not instantly propagate and therefore results in gradual stiffness degradation.

As seen in Fig. 7, none of the failures were localized and the failures occurred uniformly over the entire specimen. The shells tested with biaxial tension failed slowly. For the N420A-SBT specimen, the failure occurred over several minutes as the strains increased along the yield plateau. As the specimen was yielding the load was briefly reduced and reloaded to evaluate any degradation in stiffness and to illustrate that significant load could be carried along the yield plateau. N550B-SBT exhibited a similar response. For these members, once crushing began, marked by a significant decrease in load, the load dropped over a span of several seconds. Over this period a large amount of the concrete cover became delaminated from the core and some spalling occurred.

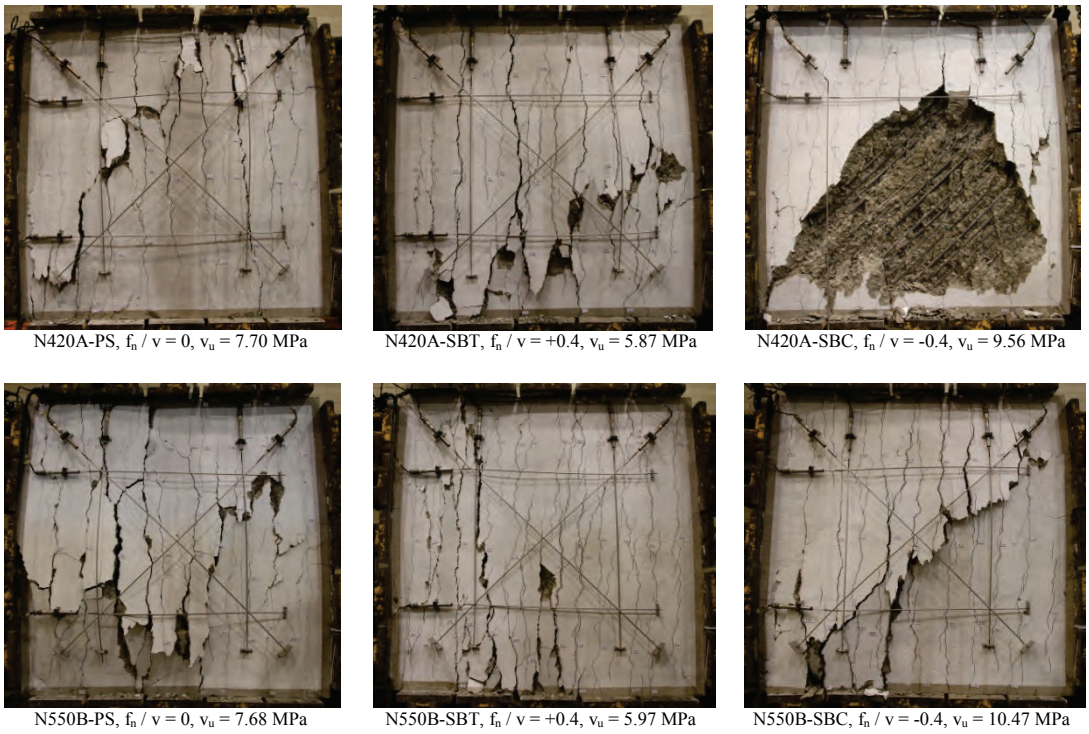

Figure 7. Photographs of shells after failure.

In contrast to the specimens subjected to biaxial tension, the members subjected to biaxial compression did not exhibit a yield plateau. As the peak load was reached the members crushed catastrophically without any visual warning of failure. For instance, N420A-SBC looked as though it was not near failure, no concrete cover had delaminated from the core and no spalling had occurred. Once the next load level was achieved (an increase of 0.1 MPa) the specimen went from looking nearly undamaged to the photograph shown Fig. 7 in a span of roughly 0.5 seconds. Nearly all the concrete cover on both

faces delaminated and spalled from the shell. N550B-SBC behaved in a similar manner. Although the concrete cover did not fall off the specimen it became completely delaminated and the reinforcing bars were visible. The reason that these members failed so abruptly is because they had very little ductility. To ensure a uniform state of stress throughout the specimen the members were loaded in force control. Once the control system is commanded to decrease the load, either manually or through a control limit that is triggered, the frame of the Shell Element Tester released stored elastic energy back into the specimen. This release destroyed the specimens in a catastrophic way because the members did not have sufficient ductility to accommodate the demand.

The specimens subjected to pure shear did not fail as abruptly as the members subjected to biaxial compression. As the peak load was approached, the strains increased quickly. Although a distinct yield plateau was not achieved, this provided some warning of failure. Once crushing ensued the failure proceeded quickly in a similar way to the members subjected to biaxial compression. The concrete cover delaminated from the core and significant spalling occurred.

CONCLUSION

The use of high-strength steel reinforcing bars, in reinforced concrete structures, lowers the ultimate shear strength of members with the same ρf_y ratio. As predicted by the MCFT, this reduction in strength results from the increased compression softening caused by the decreased steel stiffness and the reduction in tensile stresses that can be carried in the cracked concrete. Members subjected to shear and biaxial tension are weaker but more ductile than similar specimens tested in pure shear. Members subjected to shear and biaxial compression have higher strengths but fail in a brittle manner. The MCFT is accurately able to predict the ultimate strength of members with a mean test to predicted ratio of 0.992 and a coefficient of variation of 5.38%. The MCFT is also able to accurately capture the shear strains at peak stress with a mean test to predicted ratio of 0.987 and a coefficient of variation of 8.10%. As predicted, members with high-strength steel had larger crack widths than similar members with normal strength steel. Although an increase in steel strength reduces the shear strength of reinforced concrete members, this phenomenon is accurately predicted by the MCFT. The CSA code, and others that are based on the MCFT, are formulated to capture the strain effect in shear and in turn the increased compression softening effects and reduction in the amount of tension that can be carried in the cracked concrete.

ACKNOWLEDGMENTS

The authors would like to express their gratitude for the support from the Korea Institute of Energy Technology Evaluation and Planning (KETEP) funded by the Ministry of Knowledge Economy that has made this research possible (No. 2011T100200162).

REFERENCES

ACI Committee 318. (2008). *Building Code Requirements for Structural Concrete (ACI 318-08) and Commentary*, Farmington Hills, MI, USA.

Bentz, E. C., Membrane-2012, http://www.ecf.utoronto.ca/~bentz/m2k.htm. (last accessed Dec. 29, 2012)

Bentz, E. C. and Collins, M. P. (2006). "Development of the 2004 CSA A23.3 Shear Provisions for Reinforced Concrete," *Canadian Journal of Civil Engineering*, CSCE, 33(5), 521-534.

Bentz, E. C., Vecchio, F. J. and Collins, M. P. (2006). "The Simplified MCFT for Calculating the Shear Strength of Reinforced Concrete Elements," *ACI Structural Journal*, ACI, 103(4), 614-624.

BS EN 1992-1-1:2004. (2004). *Eurocode 2—Design of Concrete Structures. Part 1: General Rules and Rules for Buildings*, CEN, Brussels, Belgium.

Collins, M. P. and Mitchell, D. (1991). *Prestressed Concrete Structures*, Prentice Hall, NJ, USA, 61.

Collins, M. P., Bentz, E. C. and Sherwood, E. G. (2008). "Where is Shear Reinforcement Required? Review of Research Results and Design Procedures," *ACI Structural Journal*, ACI, 105(5), 590-600.

CSA A23.3-04. (2004). *Design of Concrete Structures*, CSA, ON, Canada.

Liping, X., Bentz, E. C. and Collins, M. P. (2011). "Influence of Axial Stress on Shear Response of Reinforced Concrete Elements," *ACI Structural Journal*, ACI, 108(6), 745-754.

Vecchio, F. J. and Collins, M. P. (1986). "The Modified Compression-Field Theory for Reinforced Concrete Elements Subjected to Shear," *ACI Structural Journal*, ACI, 83(2), 219-231.